EUROPEAN ORGANIZATION FOR NUCLEAR RESEARCH

A HIGH-INTENSITY LOW-MOMENTUM SEPARATED ANTIPROTON BEAM FOR THE STUDY OF ANNIHILATIONS AT REST

G. Bassompierre*), G. Binder, P. Dalpiaz, P.F. Dalpiaz,
M. Ferro-Luzzi, G. Gissinger, S. Jacquey, C. Peroni,
F.M. Schmitt, M.A. Schneegans*) and L. Tecchio

Institut des Sciences exactes et appliquées, Mulhouse, France
Centre national de la recherche scientifique, Strasbourg, France
Istituto di Fisica Superiore dell'Università e
Istituto Nazionale di Fisica Nucleare, Torino, Italy

ABSTRACT

The main features of the low-momentum separated antiproton beam built at the CERN Proton Synchrotron to allow the stopping of a large number of antiprotons are described. An effective stopping rate of 1000 antiprotons per 10^{12} protons on the PS internal target is obtained. Results of the measurement of the rate of reaction $\bar{p}p \to h^+h^-$ in a 50 cm long liquid hydrogen target are given to illustrate the stopping and monitoring techniques.

Geneva - 12 August 1976
(Submitted to Nuclear Instruments and Methods)

---

*) Present address: L.A.P.P., Annecy-le-Vieux, France.

1. INTRODUCTION

The aim of this paper is to describe the low-momentum enriched antiproton beam m_{14}, which is now available at CERN, in the Proton Synchrotron South Hall. This beam has been built to allow the systematic study of antiproton annihilation at rest, which is fundamental for the understanding of proton form factors in the time-like region and of $\bar{p}p$ bound states. This research was proposed[1] in 1973 and is now in progress at the CERN PS. Some preliminary results have been published[2,3].

For this study, it is essential to stop in a liquid hydrogen target the largest possible amount of antiprotons. The m_{14} beam is a two-stage low-energy electrostatically separated antiproton beam, with a large acceptance 6.4 msr, up to 900 MeV/c momentum at which a maximum number of antiprotons can be brought to rest. Most of the antiprotons transmitted by the beam optics ($\Delta p/p$ maximum = ±1.8%) can be stopped in a 50 cm liquid hydrogen target. The m_{14} beam has been built on the site of the previously existing antiproton beam m_{11} [4], which had 1.7 msr acceptance and was tunable up to 2.5 GeV/c.

In Sections 2 and 3 of this paper, we describe the beam optics and give the performance of beam m_{14}. In Section 4, the stopping of the antiprotons is explained and the measured annihilation rates are given.

2. BEAM OPTICS

The layout of the 46 m long m_{14} beam is shown in Fig. 1. It originates in the PS internal target $\hat{1}$; this is a beryllium target 1 mm high, 2 mm wide and 10 mm long, which is oriented at an angle of 160 mrad with respect to the m_{14} beam axis. Taking into account this angle, as well as the scattering of 0.9 GeV/c antiprotons through the vacuum windows, the apparent horizontal size of the target is $\sim$ 5 mm.

The mean production angle is 360 mrad, the angular acceptance is ±92 mrad horizontally and ±22 mrad vertically, yielding a 6.4 msr solid angle. The maximum transmissible momentum bite is $\Delta p/p$ = ±1.8%. The beam optics, represented in Fig. 2, basically consists of two focusing stages, in the first of which momentum selection and mass separation are performed. At the momentum collimator HC, where the horizontal focus is realized, the beam is still vertically open, and a sextupole has been associated with the collimator in order to reduce the vertical aberrations. The second stage is used for chromatic dispersion compensation, background reduction, and matching to the experimental target.

The mass separation is obtained by means of a 6 m electrostatic cavity. An electric field of 30 kV/cm applied across a 17 cm symmetric gap provides an image separation at the mass collimator VC of $\sim$ 18 cm. Compensating magnets MVS allow the beam to be brought back onto its trajectory in the vertical plane.

The elements denoted by MV are vertical bending magnets which raise the beam level by 0.685 m above the nominal 1.26 m height, as required by the unusual height of the experimental target due to the large turntable system supporting the experimental apparatus. These magnets introduce a vertical momentum dispersion at the final focus of ±1.7 mm/(±1% $\Delta p/p$). This is negligible when compared with the chromatic aberrations inherent in the large beam acceptance.

The magnifications at the experimental target T are large, because of the long focal distance from the last quadrupole (4 m): $M_h = 5.5$ and $M_v = 7$. In order to minimize losses and enlargement of the beam due to multiple scattering, the beam is transported in vacuum pipes and the window thicknesses are kept to a minimum.

Tables 1 summarizes the main features of the m_{14} beam.

3. BEAM RATES

The rates were measured by the coincidence of two counters:

- counter 1: 10 cm wide, 6 cm high, 0.5 cm thick and placed immediately behind magnet MV_2;
- counter 2: 8 cm wide, 5 cm high, 0.5 cm thick and placed at 3.35 m from counter 1 and 30 cm in front of the experimental target.

During these rate measurements, the PS was operating at 24 GeV/c with 2.6 sec cycles and 400-500 msec flat top. The beam was first tuned with positive and negative particles and no electrostatic separation, the bending magnet M_2 being set at the nominal value corresponding to the wanted momentum.

With the momentum collimator open at a maximum (±54 mm) and the mass collimator at ±20 mm, the following rates at 0.9 GeV/c were observed for 0.6×10^{12} protons on target $\hat{1}$ *):

positive particles: $\sim 4 \times 10^6$
negative particles: $\sim 2 \times 10^6$.

The separator was then set at its nominal value: 510 kV. Separation curves were performed by varying the current in the compensating magnets MVS. Figure 3 shows a separation curve obtained with a positive beam, and narrow momentum (±5 mm) and mass (±1 mm) collimators. The rate of coincidence 1*2 per 10^5 MON is plotted, where the monitor (MON) is a counter telescope monitoring the internal target $\hat{1}$ production rate. 10^5 MON correspond roughly to 4 PS bursts of 0.6×10^{12} protons on target $\hat{1}$.

---

*) With the PS booster : (3-4) $\times 10^{12}$ p/burst; (15-20)% on target $\hat{1}$.
Without the PS booster: 1.8×10^{12} p/burst; 33% on target $\hat{1}$.

In Figure 4, a separation curve with negative particles and narrow collimator settings is represented. The rate of $1*2/10^5$ MON (dots) in the antiproton region is shown on a 100-times-expanded scale. The rate of antiprotons selected by time of flight (TOF) shows a clean peak (triangles). The TOF is measured between counters 1 and 2 on a 3.35 m flight path. To obtain a clean antiproton selection, a high-low discrimination technique is used providing the best time information from each counter and allowing already some rejection of the pions. The overlap of the pulses of counters 1 and 2 is analysed in an analogue-to-digital converter and recorded on tape. A fast antiproton signal for the electronic trigger is obtained by transforming the length of the overlap pulse of counters 1 and 2 in pulse height by a clipping method. A resolution of ±0.5 nsec is achieved and the pion contamination is brought down to a few per cent.

The rates of $\pi^- + \bar{p}$ and of $\bar{p}$ selected by TOF, when the compensating magnets are set on the antiproton peak, are shown in Fig. 5 as a function of the mass collimator width for a maximum momentum collimator width (±54 mm). For ±20 mm, the observed $\pi^-/\bar{p}$ ratio is around 10 and there is little gain in antiproton rate with a wider opening.

A separation curve at 0.9 GeV/c in the antiproton region is shown in Fig. 6 with the chosen collimator conditions:

HC: ±54 mm ($\Delta p/p = \pm 1.8\%$)
VC: ±20 mm.

The observed antiproton rate (in 5.5 PS bursts) corresponds, after background subtraction, to 10,000 $\bar{p}$ per 10^{12} protons on target $\hat{1}$.

The antiproton yield measured as a function of the beam momentum, with the nominal collimator settings, is shown in Fig. 7. The errors are mainly due to background subtraction and uncertainties in target $\hat{1}$ sharing. The apparent flattening of the $\bar{p}$ rate observable at 950 MeV/c is due to the saturation of some beam-transport elements.

The image of the beam in the experimental target region, at 0.9 GeV/c and with the nominal collimator settings, was scanned to be 8 cm horizontally by 3 cm vertically.

The relevant parameters of the beam and measured rates are summarized in Table 2.

4. STOPPING OF THE ANTIPROTONS

4.1 Beam telescope

The maximum momentum bite ($\Delta p/p = \pm 1.8\%$) of the m_{14} beam corresponds to a length of liquid hydrogen, in which the antiprotons can be brought to rest, of

about 40 cm. If we allow for straggling, a 50 cm long target contains most of the stopped antiprotons. This length was considered as a maximum compatible with the size of the 4π geometry apparatus used for our experiment[1]. A diameter of 15 cm was chosen to allow for the increase of image size and the beam divergence caused by the moderator. The target dimensions and structure are shown in Fig. 8. The walls and ends of the appendix are made of 0.25 mm thick mylar, surrounded by 40 sheets of 6 μ aluminized mylar for isolation. An evacuated, 5 mm thick, dellite tube closed at both ends by 0.25 mm mylar windows surrounds the appendix. The 9 ℓ target is connected to a tower container of 18 ℓ, which guarantees by a permanent circulation of the liquid hydrogen a good filling of the appendix. Transfer from a dewar container occurs about every 10 h.

Counters 1 and 2, used to select electronically antiprotons, are followed by a moderator as shown in Fig. 9. A lead moderator was chosen both for its low antiproton attenuation factor and for its compactness yielding best stopping geometry. Just behind the moderator, counter 3 (1 cm thick) provides dE/dx measurement. A discrimination on its pulse height allows the rejection of pions which escaped the TOF selection and most antiprotons having annihilated in the moderator. Counter 4 is thin (1 mm) on a 4 mm plexiglas backing and rejects most antiprotons which annihilated in counter 3.

Counter $\bar{A}$ vetoes any event in which secondaries are produced at large angle in the moderator. Counter $\bar{Q}$ at the rear and the cylindrical counter $\bar{V}$ surrounding the target cause anticoincidence of the protons which did not stop in the target.

4.2 Trapped antiprotons

By "trapped" antiproton, we mean an antiproton penetrating into the liquid hydrogen target and not coming out. It can annihilate in flight or at rest.

Range curves and measurements of the trapped antiproton rate were performed at several momenta to find the best compromise between antiproton rate and annihilation loss. A typical range curve using protons of 900 MeV/c is shown in Fig. 10. The rate of protons emerging from the lead (TOF*3*4*$\bar{A}$) and the rate of protons stopped in the liquid hydrogen target (TOF*3*4*$\bar{A}$*$\bar{V}$*$\bar{Q}$), normalized to the number of incoming protons selected by TOF, are plotted as a function of the lead thickness. The momentum collimator was fully open to accept $\Delta p/p = \pm 1.8\%$. The curve shows that 11.5 cm of lead are necessary to bring protons of average momentum 900 MeV/c down to momenta between 230 and 420 MeV/c (28-90 MeV kinetic energy) which will penetrate into the liquid hydrogen by 5 and 45 cm, respectively, if straggling is neglected. The observed FWHH of the peak at 11.5 cm lead thickness is 12 mm, corresponding to about 50 cm of liquid hydrogen. For each thickness of lead, the discriminator levels of counters 3 and 4 were adjusted to accept the protons, but to reject most annihilations in the lead when antiprotons are used.

From this range curve, it can be seen that (24.5 ± 0.5)% of the protons selected by TOF are stopped in the liquid hydrogen. On the other hand, the rate of TOF*3*4*$\bar{A}$ was measured on several occasions for protons and for antiprotons with an empty target, with 11.5 cm of lead, and found to be:

$$N_p/TOF = (34 \pm 1)\% \quad \text{and} \quad N_{\bar{p}}/TOF = (20 \pm 0.5)\% \ .$$

The difference between N_p and $N_{\bar{p}}$ is due to the loss by annihilation in the lead for antiprotons. From the ratio

$$N_{\bar{p}}/N_p = 0.59 \pm 0.02$$

and from the fraction of protons stopped in the target, the number of antiprotons trapped (TR) in the liquid hydrogen, with respect to the incoming antiprotons selected by TOF, can be deduced:

$$TR = (14.5 \pm 0.7)\% \ .$$

This amount includes the antiprotons which will actually stop inside the target and those which will annihilate in flight in the liquid hydrogen.

The fraction TR can be determined in a direct, but less accurate, way by measuring the ratio TOF*3*4*$\bar{A}$*Q/TOF with an empty target. Here, counter Q (55*55 cm^2) in coincidence defines approximately the solid angle of the antiprotons which emerge from the lead and pass through a length of target sufficient to stop them when the target is full. This ratio was measured at several momenta and is plotted in Fig. 11. The errors are mainly due to the uncertainties in range adjustment and in threshold settings on the pulses of counters 3 and 4. The absolute trapped antiproton rate as a function of antiproton momentum is also represented; it shows a clear maximum around 900 MeV/c, even if the antiproton rate at 950 MeV/c extrapolated from the steep part of the production curve is used (see Fig. 7). From TR at 900 MeV/c, we derive that between 800 and 900 antiprotons per burst are trapped in the liquid hydrogen target in standard PS and target $\hat{1}$ conditions.

4.3 Antiproton stopping rate

In order to determine the fraction of antiprotons annihilating in flight in our 50 cm long target in the previously defined beam conditions, we measured the rate of the reaction

$$\bar{p}p \rightarrow hh, \quad \text{where hh is } \pi^+\pi^- \text{ or } K^+K^- \ .$$

The annihilations into hh were detected in a system of four blocks of scintillators and optical spark chambers described elsewhere[2,3]. Photographs were taken only when two charged particles were detected in opposite detectors, excluding gamma-rays in the other detectors. Events showing anything other than the two charged tracks were rejected on the pictures. The directions of the tracks in the thin-foil optical spark chambers were measured and reconstructed in space; the

distribution of the opening angles between the two hadrons is plotted in Fig. 12. A clear peak in the collinear region (around 180°) allows an unambiguous selection of the events corresponding to annihilations at rest into hh. The excess of events in the forward region (with respect to the incoming beam direction), between 153° and 171°, corresponds to hh produced by antiprotons annihilating in flight between 150 and 450 MeV/c.

In fact, if we decrease the many-body background by requiring coplanarity within ±10° between the annihilation products and the incoming antiproton, we obtain the opening angle spectrum shown in Fig. 13. The longitudinal distribution of the vertices in the 50 cm target is represented in Fig. 14 for the collinear hh events. No cut is applied on the target length. It confirms that 50 cm of liquid hydrogen contain most of the effectively stopped antiprotons.

The number of hh events observed in the opening angle spectra is 220 at rest and 80 in flight, corresponding to 5.12×10^6 antiprotons in the 900 MeV/c beam. If we assume the branching ratio

$$B_{hh} = \frac{\Gamma(\bar{p}p \rightarrow hh)}{\Gamma(\bar{p}p \rightarrow \text{total})}$$

to be approximately constant between 500 MeV/c and zero antiproton momentum, we can derive B_{hh} from the total number of observed events, since

$$N_{hh} = N_{\bar{p}} * \varepsilon * TR * B_{hh} ,$$

where ε is the total efficiency of our apparatus for hh detection and TR the fraction of antiprotons trapped in the target as determined in Section 4.3. We obtain

$$B_{hh} = (0.43 \pm 0.05)\% .$$

This value is in excellent agreement with the data of Baltay et al.[5] for $\pi^+\pi^-$ and K^+K^-.

We can determine the fraction of antiprotons annihilating in flight from the amount of events observed in the hh channel in flight and at rest

$$AF = \frac{80}{80 + 220} = (27 \pm 4)\% ,$$

which means that the 14.5% antiprotons trapped in the target divide into (3.9 ± 0.6)% annihilating in flight and (10.6 ± 1.6)% effectively stopping.

A value of AF can also be derived from the antiproton spectrum measured by time of flight just in front of the target. Multiplying this spectrum by the probability of annihilation in flight, calculated following Bognadova et al.[6] with the assumption of a smooth $1/\beta$ annihilation cross-section behaviour, we obtain AF = (30 ± 5)% in good agreement with the value deduced from the observed hh events.

These data are summarized together with beam m_{14} parameters and rates in Table 2.

Acknowledgements

We wish to thank M. Croissiaux and M.I. Ferrero for their continuous support, C. Franzinetti for his contribution at the early stages and P.I.P. Kalmus for interesting discussions. The successful design of the beam is due in great part to G. Petrucci. We are grateful to the MPS separator group for the reliable operation of the electrostatic separator and to the MPS survey group for the accurate alignment of the beam. We particularly wish to thank P. Alivon, F. Bastari, G. Bochaton, G. Bonfillou, L. Mazzone and G. Novellini for the construction and efficient operation of our liquid hydrogen targets. We also wish to thank our technicians G. Abbrugiati, S. Janet and A. Pia for their work on the beam telescope construction.

REFERENCES

1) G. Bassompierre, P. Dalpiaz, P.F. Dalpiaz, M.I. Ferrero, C. Franzinetti, G. Maderni, M. Maringelli and M.A. Schneegans, A systematic study of electron pair production in $\bar{p}p$ annihilation at rest, Proposal PH I/COM-73/3, January 1973.

2) G. Bassompierre, G. Binder, P. Dalpiaz, P.F. Dalpiaz, G. Gissinger, S. Jacquey, C. Peroni, M.A. Schneegans and L. Tecchio, Measurement of the branching ratio $\Gamma(\bar{p}p \to e^+e^-)/\Gamma(\bar{p}p \to \text{total})$ in antiproton-proton annihilation at rest, submitted to Phys. Letters (July 1976).

3) G. Bassompierre, G. Binder, P. Dalpiaz, P.F. Dalpiaz, G. Gissinger, S. Jacquey, C. Peroni, A. Ruzza, M.A. Schneegans and L. Tecchio, Evidence for the production of heavy vector mesons in antiproton-proton annihilation at rest, submitted to Phys. Letters (July 1976).

4) P.I.P. Kalmus, E. Eisenhandler, W.R. Gibson, C. Hojvat, L.C.Y. Lee Chi Kwong, T.W. Pritchard, E.C. Usher, D.T. Williams, M. Harrison, W.H. Range, M.A.R. Kemp, A.D. Rush, J.N. Woulds, G.T.J. Arnison, A. Astbury, D.P. Jones and A.S.L. Parsons, Low-momentum antiproton production at the CERN Proton Synchrotron, CERN 71-25 (1971).

5) C. Baltay, P. Franzini, G. Lutjens, J.C. Severiens, D. Tycho and D. Zannello, Phys. Rev. 145, 1103 (1966).

6) L.M. Bogdanova, O.D. Dalkarov, B.O. Kerbikov and I.S. Shapiro, Narrow $N\bar{N}$ resonances, ITEP-27, Moscow (1975).

Table 1

m_{14} main parameters

Beam length from internal to experimental target		46 m
Production angle		360 mrad
Maximum design momentum		0.9 GeV/c
Angular acceptances	$\alpha_h \simeq \pm 92$ mrad, $\alpha_v \simeq \pm 22$ mrad	
Solid angle acceptance		6360 μsr
Maximum transmissible momentum bite		$\Delta p/p = \pm 1.8\%$
Electrostatic separator:		
Total length of electrodes		6 m
Gap		17 cm
Field		30 kV/cm
At the momentum collimator:		
Horizontal magnification		-9
Momentum dispersion		30 mm/(1% $\delta p/p$)
Chromatic aberrations		±13 mm/(±1% $\delta p/p$)
At the mass collimator:		
Vertical magnification		-8.8
Vertical chromatic aberration		±24 mm/(1% $\delta p/p$)
Image separation between π and p at 0.9 GeV/c		185 mm
At the experimental focus:		
Magnification	horizontal = 5.5	vertical = 7
Divergences (for ±1% $\delta p/p$)	$D_h \simeq \pm 16$ mrad	$D_v \simeq \pm 6$ mrad
Chromatic aberrations	$\delta_h \simeq \pm 9$ mm	$\delta_v \simeq \pm 19$ mm

Table 2

m_{14} performance under average PS conditions

PS energy: 22, 24 or 26 GeV/c	
PS intensity: without Booster: 1.8×10^{12} p/burst	
with Booster: $(3\text{-}4) \times 10^{12}$ p/burst	
Percentage on $\hat{1}$: 33% without, (15-20)% with Booster	
Available protons: 0.6×10^{12}/burst	
Beam momentum: 900 MeV/c	
Momentum acceptance: $\Delta p/p = \pm 1.8\%$	
Mass collimators: ±20 mm	
Antiproton rate: $\sim$ 6000/burst	
Ratio $\pi^-/\bar{p}$: $\sim$ 10	
Moderator: 11.5 cm Pb	
Target: 50 cm of liquid hydrogen	
Trapped antiprotons $\sim$ 850/burst:	TR = (14.5 ± 0.7)%
Stopped antiprotons $\sim$ 600/burst:	ST = (10.5 ± 1.6)%
Antiprotons annihilating in flight:	AF = (27 ± 4)%

Figure captions

Fig. 1 : Layout of beam m_{14}.

Fig. 2 : Optics of beam m_{14}.

Fig. 3 : Separation curve with a positive beam of 0.9 GeV/c. The current in the separator compensating magnets is varied. The rate in telescope 1*2 is plotted per 10^5 MON, where MON is the internal target $\hat{1}$ monitor. 10^5 MON correspond to 4-5 PS bursts of 0.6×10^{12} protons on target $\hat{1}$.

Fig. 4 : Separation curve with a negative beam of 0.9 GeV/c and narrow collimators. In the antiproton region, the 1*2 rate (dots) is shown on a 100 times expanded scale. The rate of antiprotons selected by TOF shows a clean peak (triangles and right-hand scale).

Fig. 5 : Rate of 1*2 ($\pi^- + \bar{p}$) and of TOF ($\bar{p}$) plotted as a function of the vertical collimator VC. The ratio $\pi^-/\bar{p}$ (triangles) can be read on the right-hand scale.

Fig. 6 : Separation curve at 0.9 GeV/c in the antiproton region with nominal collimator settings. Here 10^5 MON correspond to 5.5 PS bursts.

Fig. 7 : Antiproton yield as a function of momentum.

Fig. 8 : Liquid hydrogen target. All lengths and thicknesses are indicated in mm.

Fig. 9 : Beam telescope. Counters Q and V represented are used in anticoincidence when range curves are performed with protons and when neutral annihilation products are studied.

Fig. 10 : Range curve with 900 MeV/c protons.

Fig. 11 : Fraction of antiprotons trapped in the target (squares) with respect to incoming antiprotons. Trapped means in fact not coming out of the target; these antiprotons are actually stopped or annihilate in flight in the liquid hydrogen. The absolute trapped antiproton rates (open circles) are read on the right-hand scale.

Fig. 12 : Distribution of the opening angles between two hadrons.

Fig. 13 : Opening angle distribution for coplanar events.

Fig. 14 : Distribution of the reconstructed annihilation points along the beam line for collinear events.

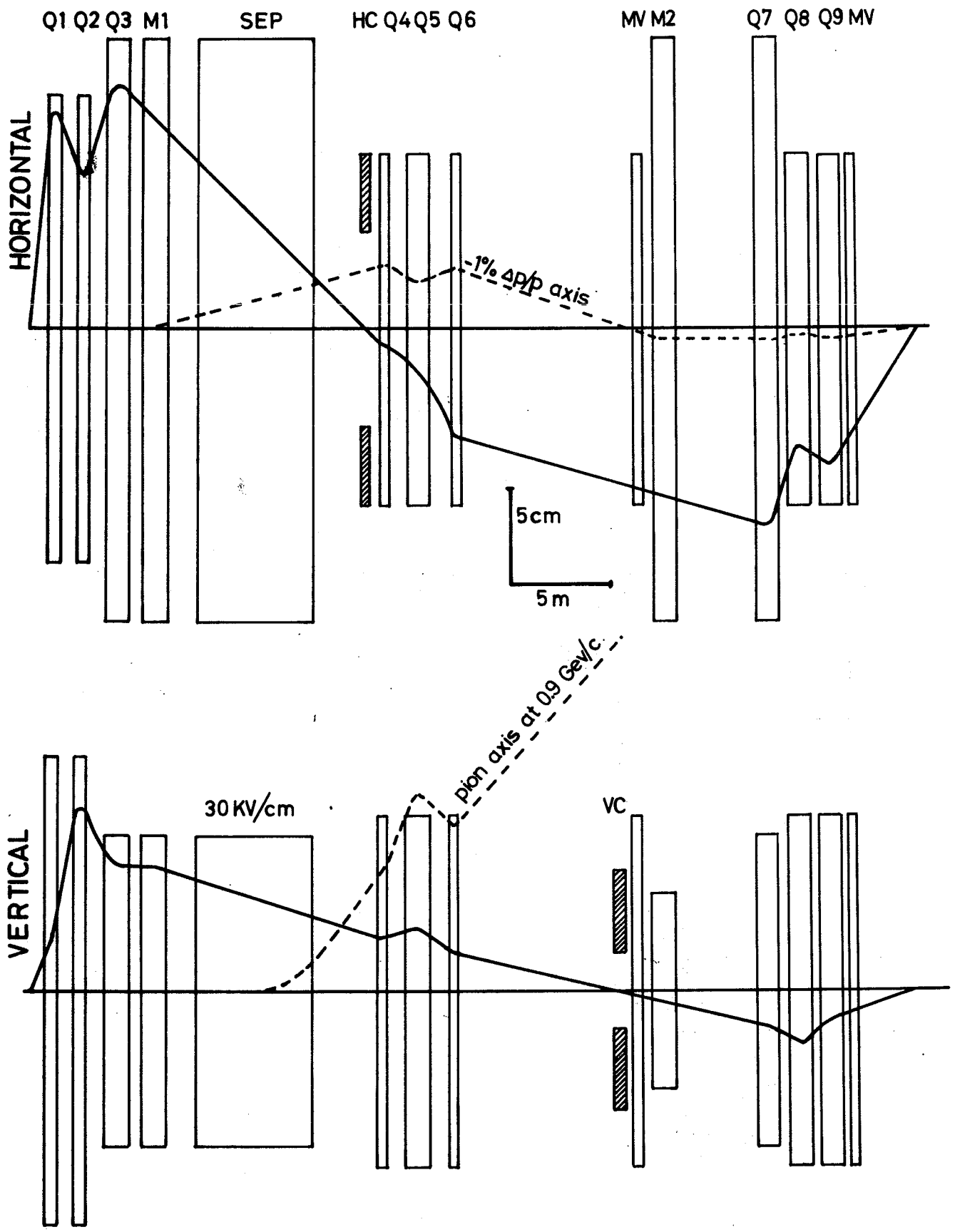
Q1 Q2 Q3 M1
SEP
HC Q4 Q5 Q6
MV M2
Q7 Q8 Q9 MV
HORIZONTAL
1% Δp/p axis
5cm
5m
pion axis at 0.9 Gev/c
30 KV/cm
VC
VERTICAL

Fig. 2

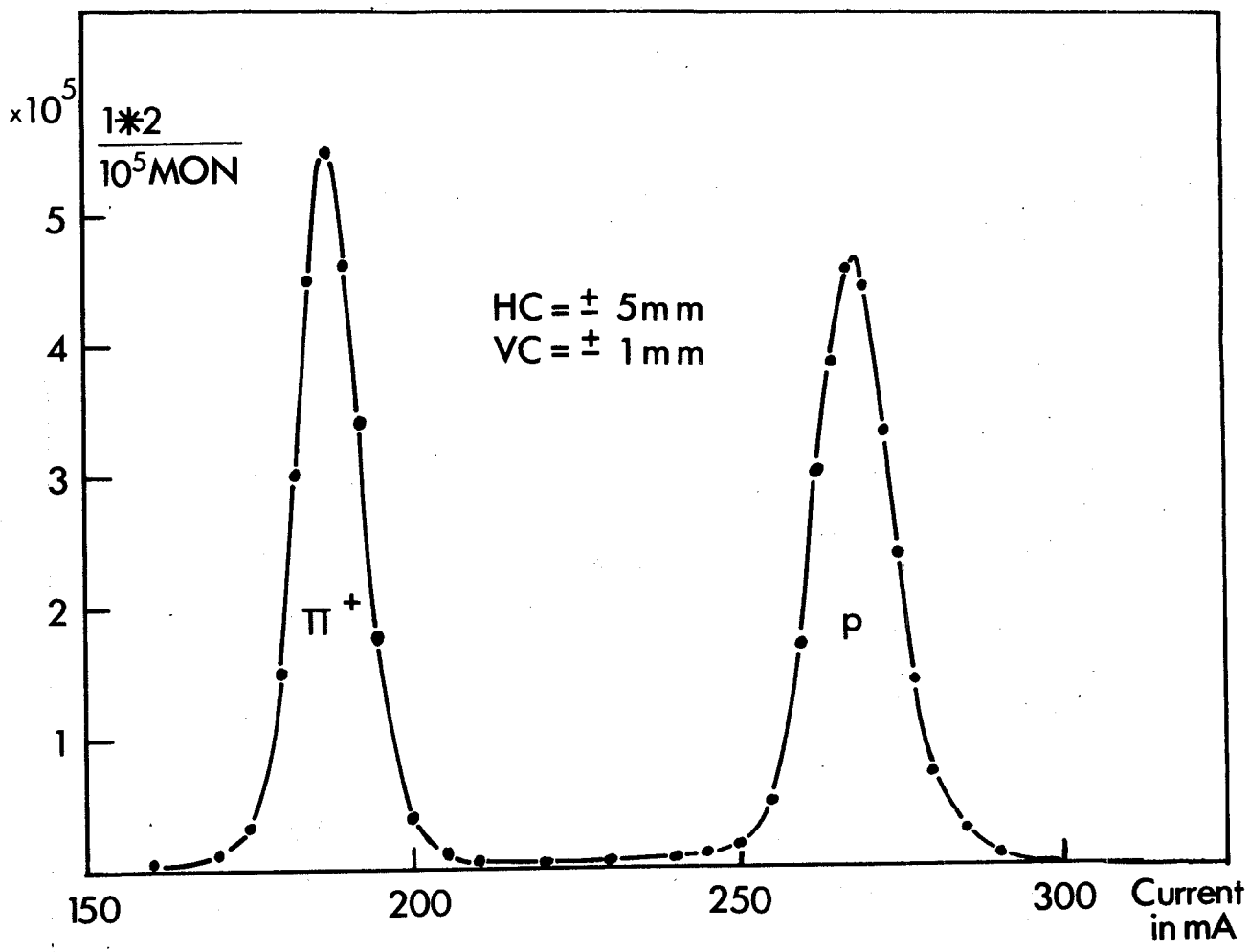
x10^5
1*2
10^5MON
5
4
3
2
1
HC = ± 5mm
VC = ± 1mm
π +
p
150
200
250
300
Current
in mA

Fig. 3

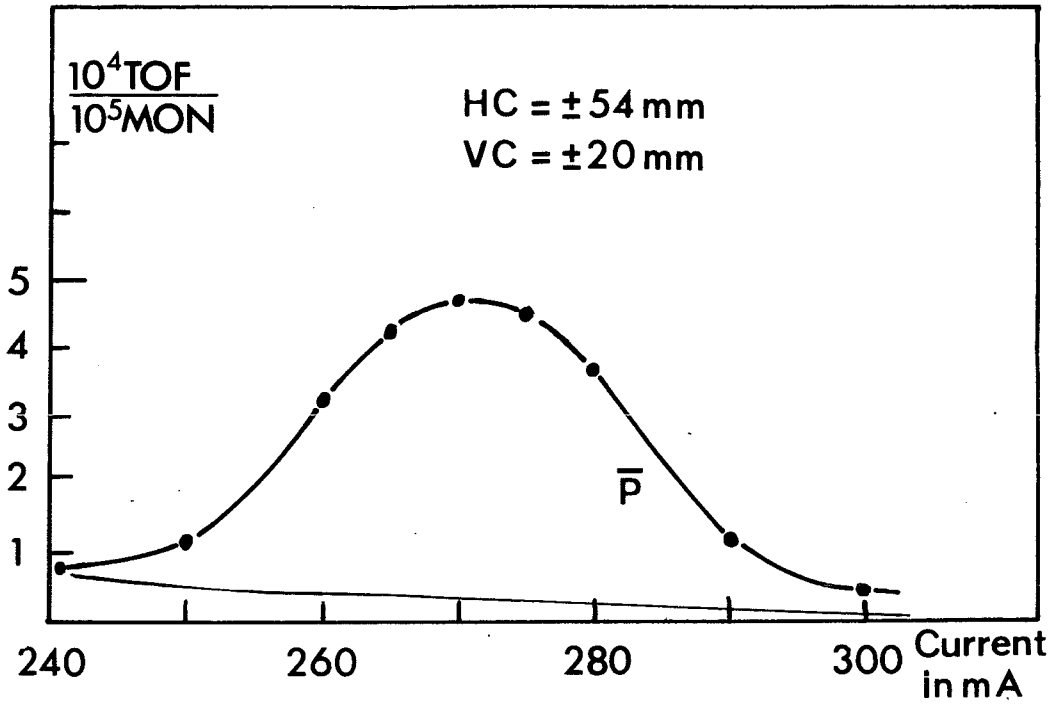
10^4TOF
10^5MON
HC = ±54 mm
VC = ±20 mm
5
4
3
2
1
$\bar{p}$
240
260
280
300
Current in mA

Fig. 6

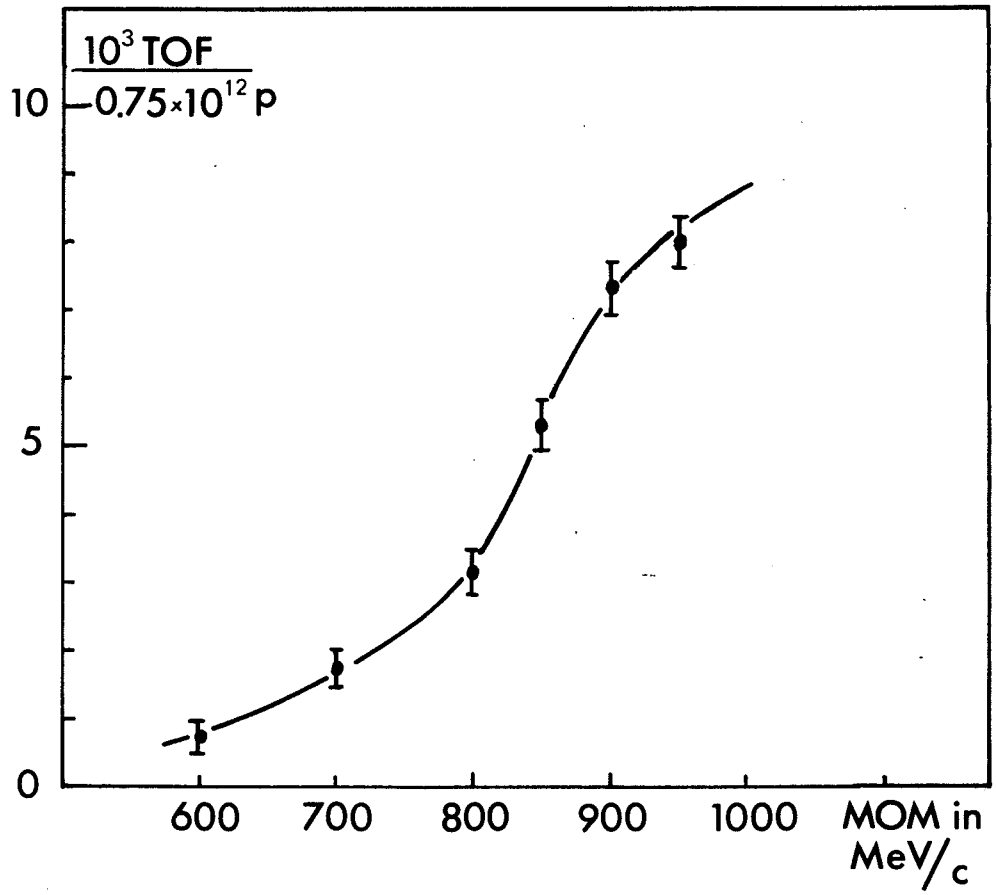
10^3 TOF
0.75×10^{12} p
10
5
0
600
700
800
900
1000
MOM in MeV/c

Fig. 7

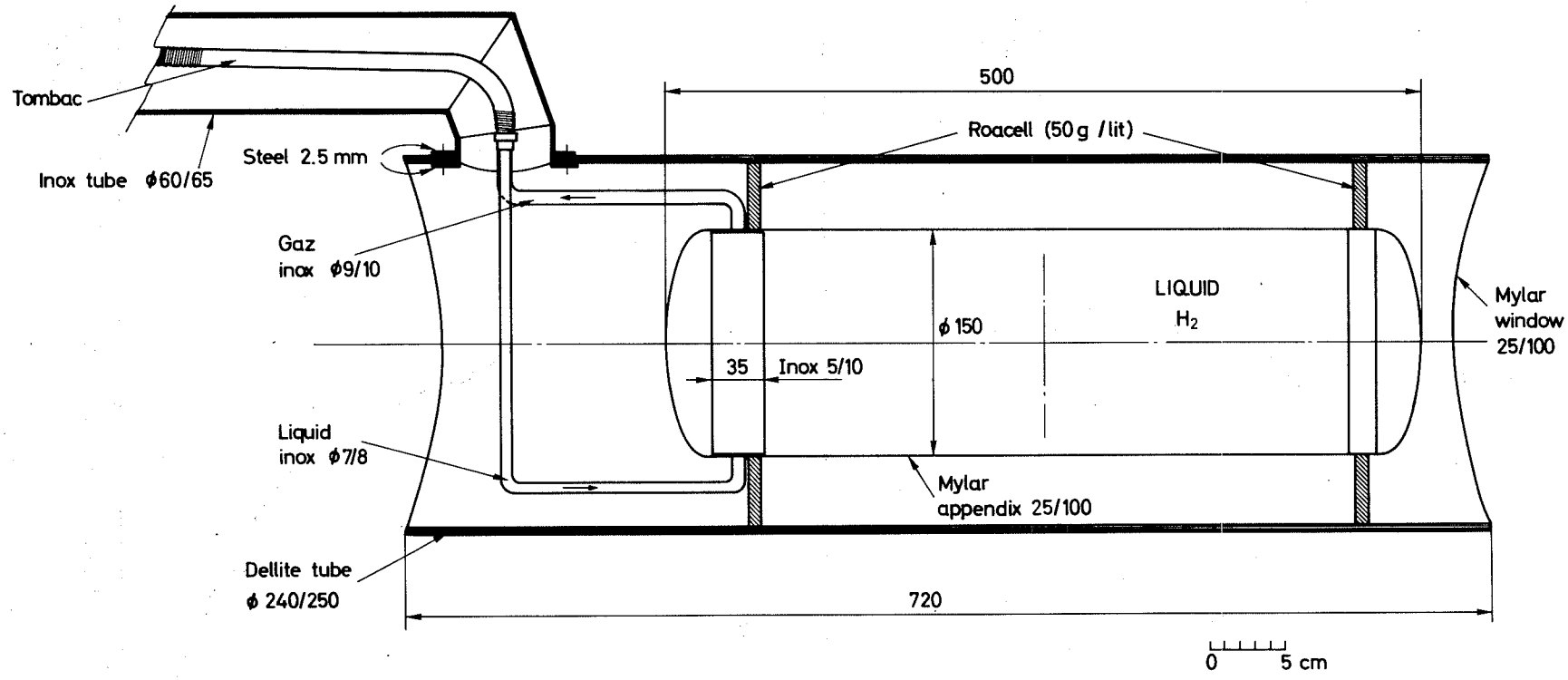
Tombac
Inox tube ϕ60/65
Steel 2.5 mm
Gaz
inox ϕ9/10
Liquid
inox ϕ7/8
Dellite tube
ϕ 240/250
500
Roacell (50 g /lit)
LIQUID
H_2
ϕ 150
35
Inox 5/10
Mylar
appendix 25/100
Mylar
window
25/100
720
0
5 cm

Fig. 8

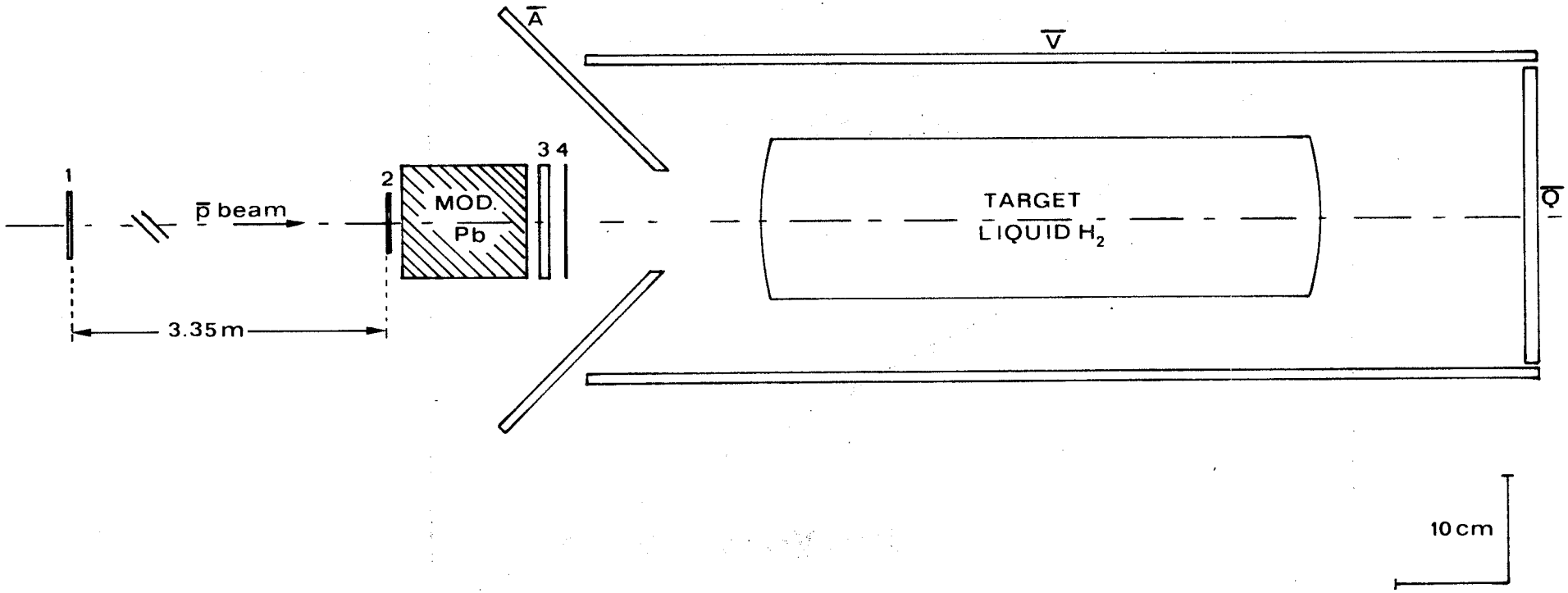

Fig. 9

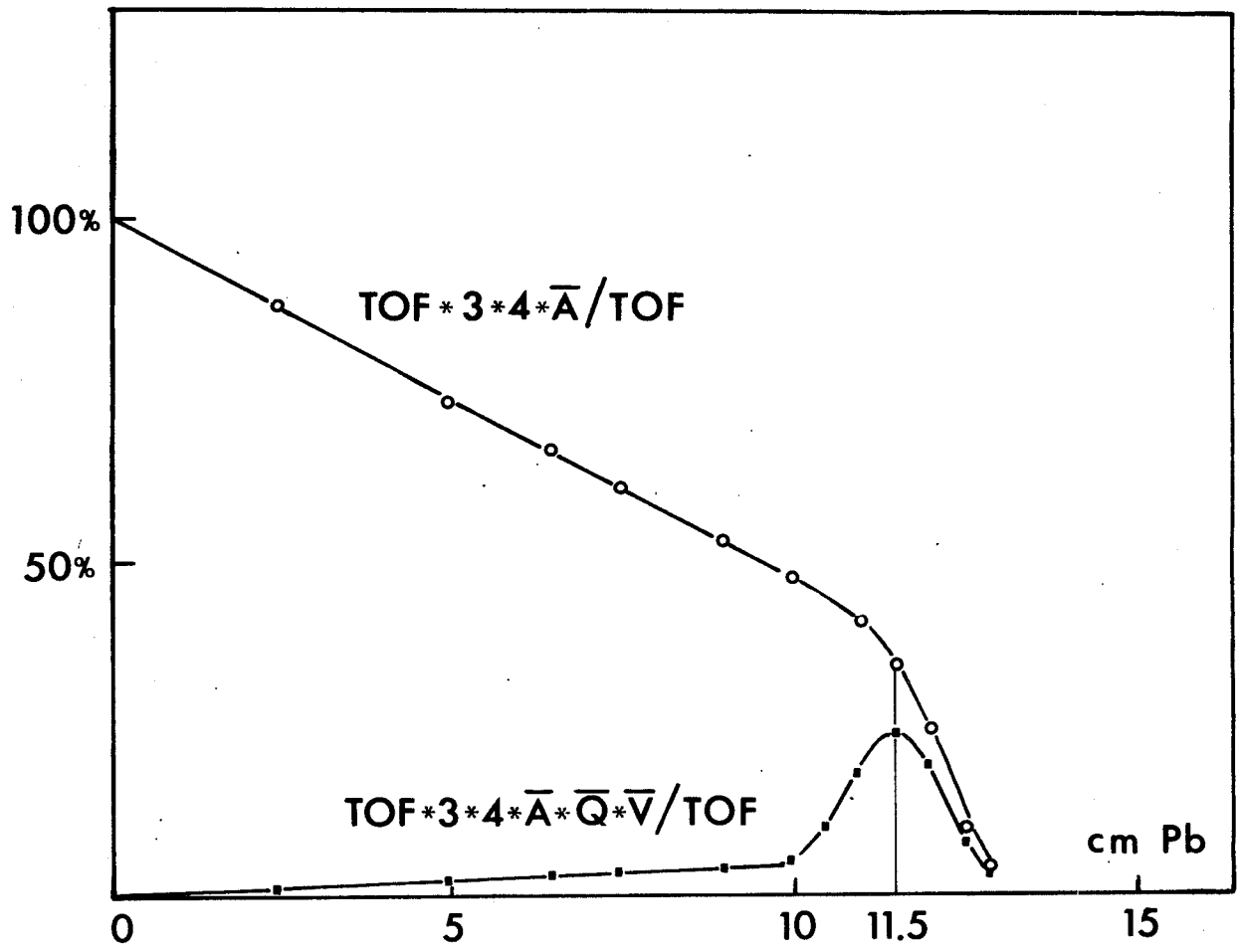
100%
50%
TOF * 3 * 4 * $\overline{A}$ / TOF
TOF * 3 * 4 * $\overline{A}$ * $\overline{Q}$ * $\overline{V}$ / TOF
cm Pb
0
5
10
11.5
15

Fig. 10

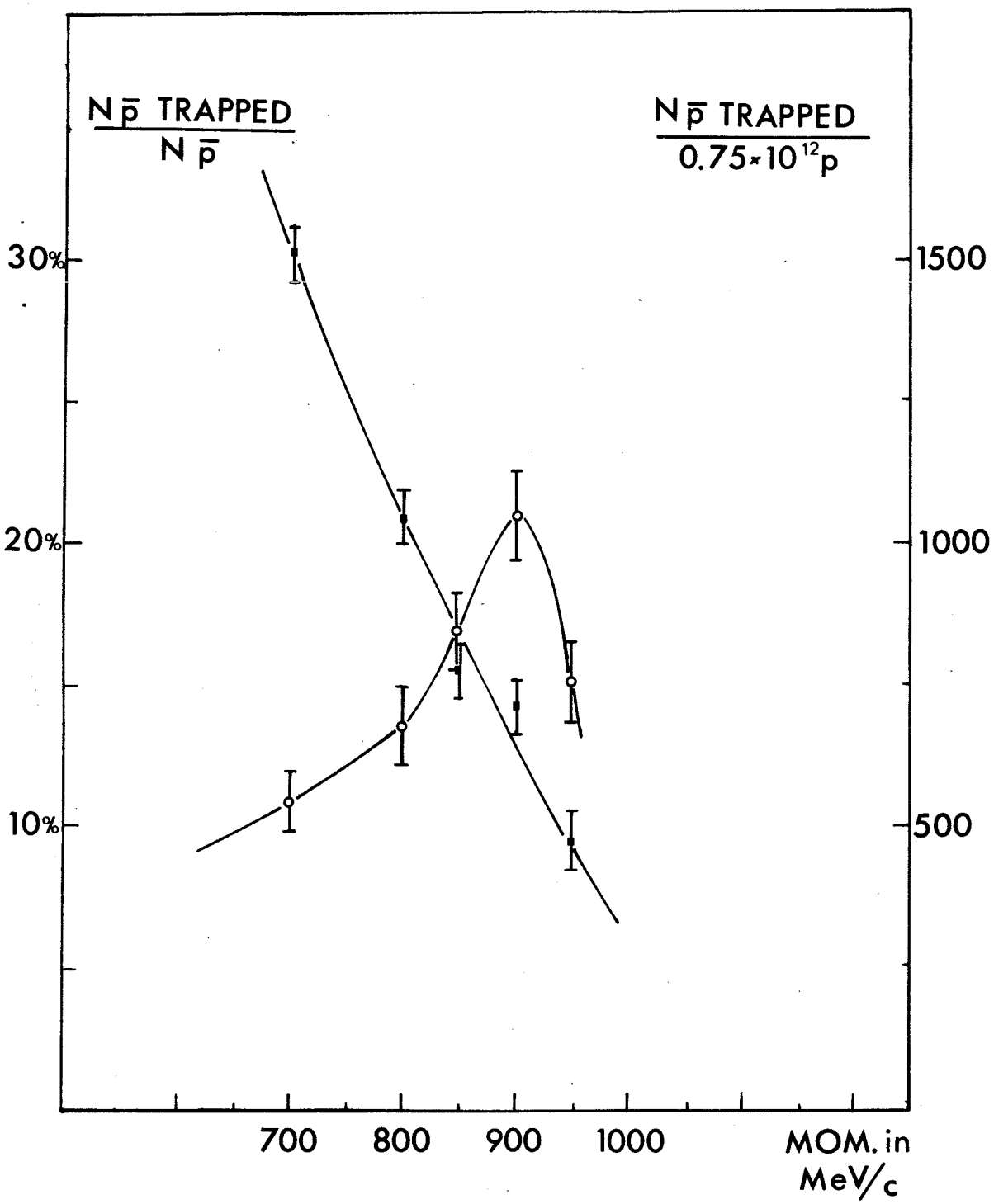
N p̄ TRAPPED / N p̄
N p̄ TRAPPED / 0.75×10^12 p
30%
20%
10%
1500
1000
500
700
800
900
1000
MOM. in MeV/c

Fig. 11

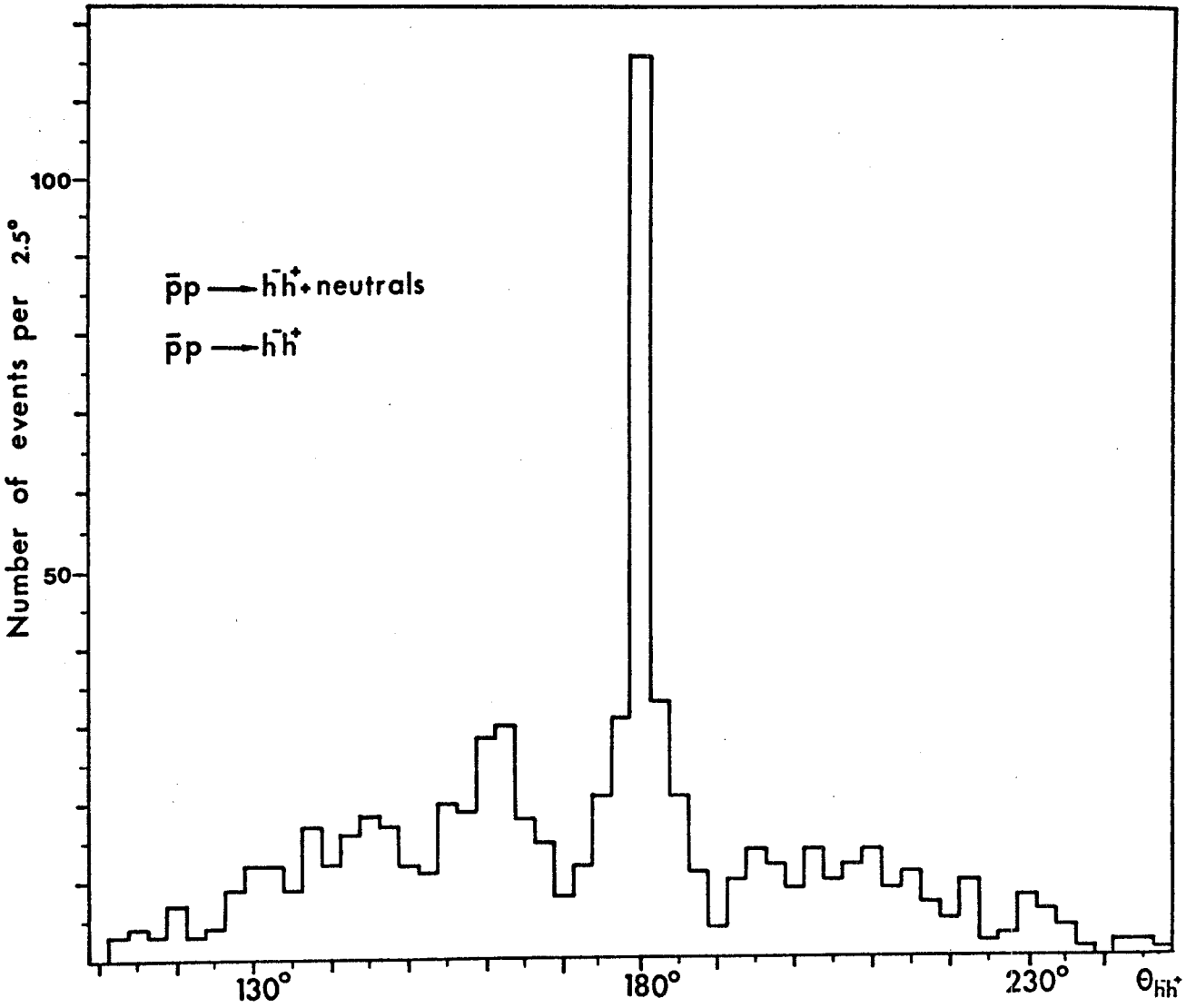
Number of events per 2.5°
100
50
$\bar{p}p \longrightarrow h^-h^+$ + neutrals
$\bar{p}p \longrightarrow h^-h^+$
130°
180°
230°
$\theta_{h^-h^+}$

Fig. 12

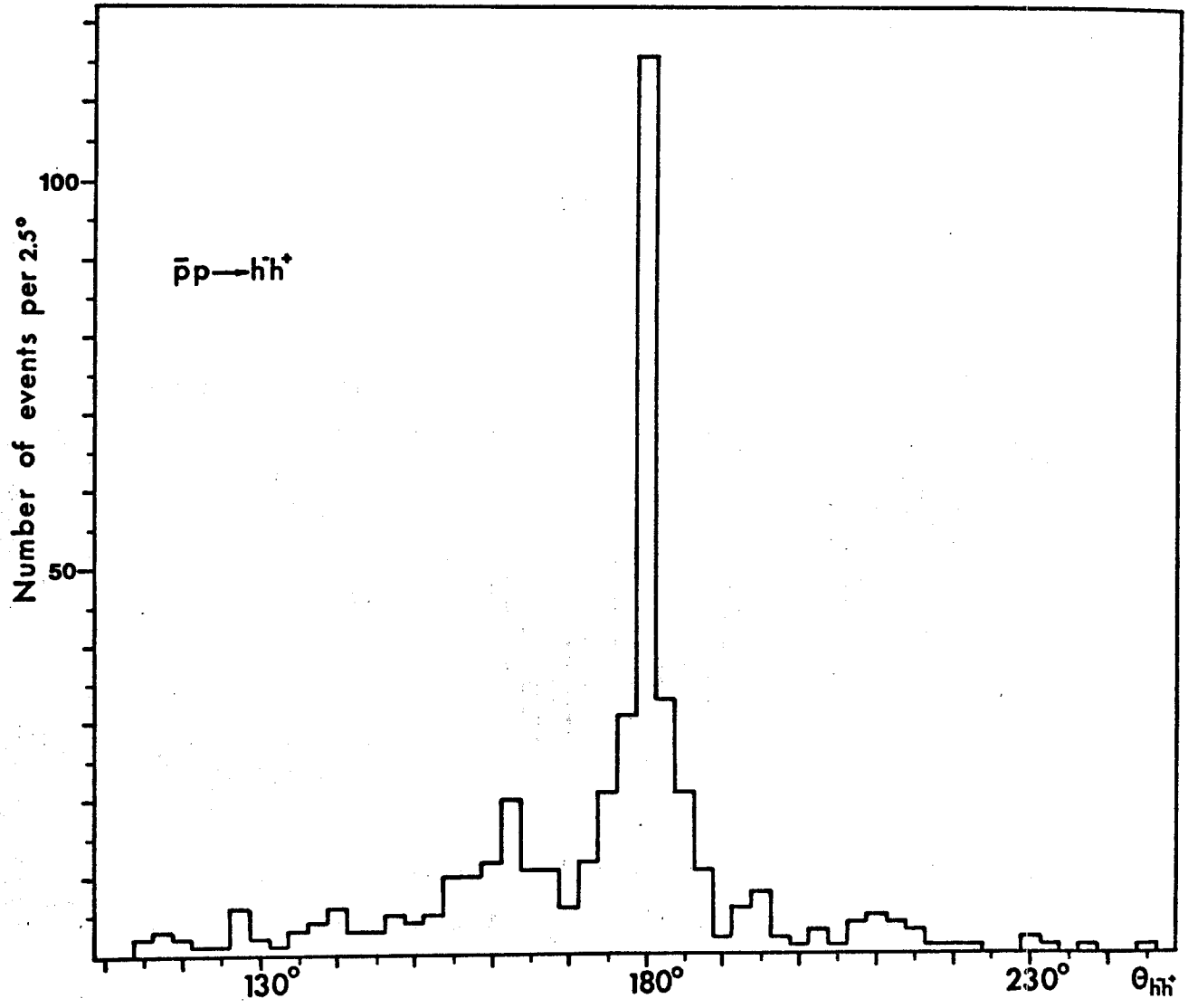
Number of events per 2.5°
100
50
$\bar{p}p \rightarrow h^-h^+$
130°
180°
230°
$\theta_{h^-h^+}$

Fig. 13

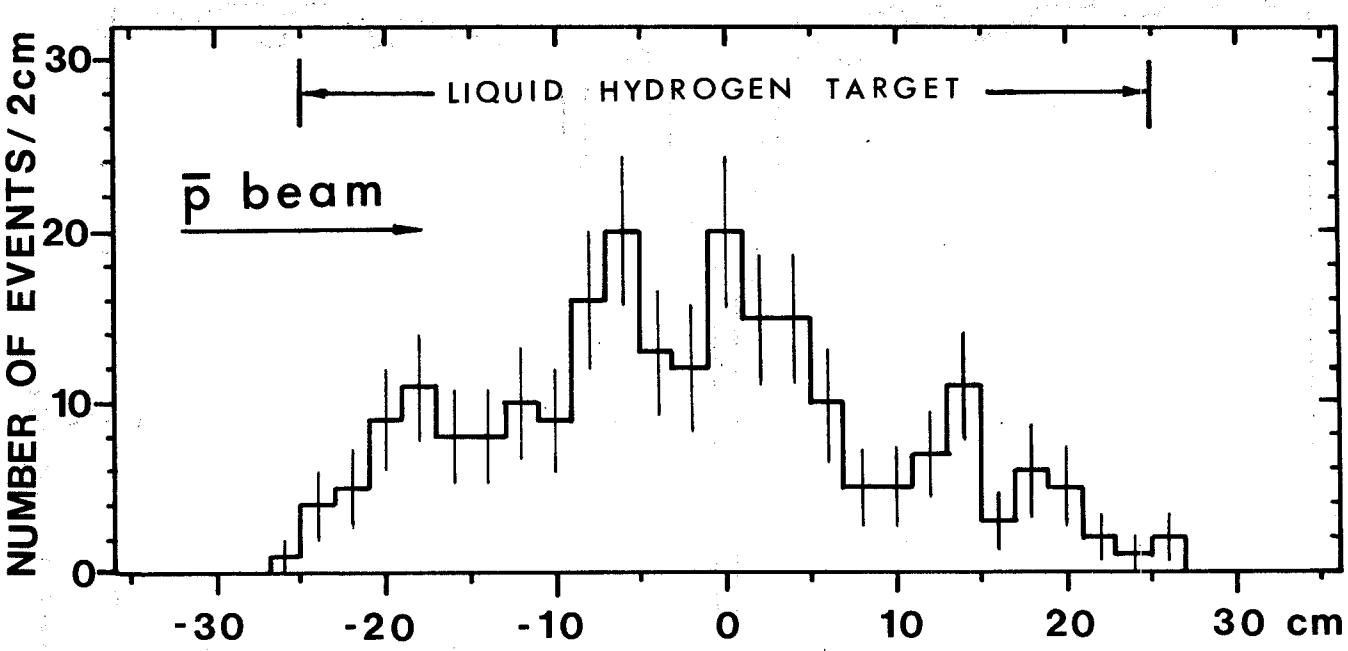
LIQUID HYDROGEN TARGET
p̄ beam
NUMBER OF EVENTS/ 2cm
30
20
10
0
-30
-20
-10
0
10
20
30 cm

Fig. 14